Available online at www.sciencedirect.com
ScienceDirect
Journal of Magnetic Resonance 190 (2008) 165–170
JMR Journal of Magnetic Resonance
www.elsevier.com/locate/jmr

Communication

Proton-detected separated local field spectroscopy

Chin H. Wu, Stanley J. Opella *

Department of Chemistry and Biochemistry, 9500 Gilman Drive, University of California, San Diego, La Jolla, CA 92093-0307, United States

Received 8 August 2007; revised 29 September 2007
Available online 10 October 2007

Abstract

PISEMO, a separated local field experiment that can be performed with either direct ^{15}N (or ^{13}C) detection or indirect ^{1}H detection, is demonstrated on a single crystal of a model peptide. The ^{1}H signals modulated by ^{1}H–^{15}N heteronuclear dipole–dipole couplings are observed stroboscopically in the windows of the multiple-pulse sequence used to attenuate ^{1}H–^{1}H homonuclear dipole–dipole couplings. ^{1}H-detection yields spectra with about 2.5 times the signal to noise ratio observed with ^{15}N-detection under equivalent conditions. Resolution in both the ^{15}N chemical shift and ^{1}H–^{15}N heteronuclear dipole–dipole coupling dimensions is similar to that observed with PISEMA, however, since only on-resonance pulses are utilized, the bandwidth is better.

Keywords: PISEMA; PISEMO; Multiple-pulse; Double-resonance; Crystal

The sensitivity advantages of indirect ^{1}H-detection in double-resonance solid-state NMR experiments are well known [1]. However, its implementation has lagged, largely because of the difficulty in devising experiments that combine continuous detection of high resolution ^{1}H chemical shift spectra with the high sensitivity required for studies of proteins at high fields. In a way, this reinforces the motivation for the original development of proton-enhanced nuclear induction spectroscopy [2], where the direct detection of ^{1}H decoupled ^{15}N (or ^{13}C) spectra obviated the difficulties of multiple-pulse line narrowing [3] required to observe high resolution ^{1}H chemical shift spectra. Many aspects of ^{1}H-detection of ^{15}N signals in solid-state NMR experiments have been discussed as part of applications of MAS solid-state NMR to polycrystalline peptides and proteins [4–9]. Initial applications of ^{1}H-detection to stationary powder samples provided essential background, [10,11]. In this Communication we demonstrate a multiple-pulse based SLF (separated local field) [12] experiment that can be performed with either direct ^{15}N-detection or indirect ^{1}H-detection. In the spectra obtained from the same amount of time and under equivalent experimental conditions on the same sample, the ^{1}H-detected signals are about 2.5 times larger than the ^{15}N-detected signals with the same noise levels. We refer to this experiment as PISEMO (polarization inversion spin exchange-modulated observation). Its resolution and sensitivity are similar to those of PISEMA (polarization inversion spin exchange at the magic angle) [13], but it has improved bandwidth, which is an important advantage for high field experiments.

SLF is among the most elegant NMR methods [12]; it yields two-dimensional NMR spectra where frequency splittings that are resolved by differences in the chemical shift frequencies of ^{15}N (or ^{13}C) nuclei provide direct measurements of the heteronuclear ^{1}H–^{15}N (or ^{1}H–^{13}C) dipole–dipole couplings. In the initial experimental implementations of SLF spectroscopy [14,15], the heteronuclear dipole–dipole couplings of interest evolve under conditions where the interfering homonuclear ($^{1}H/^{1}H$) dipole–dipole couplings are suppressed with multiple-pulse [3] irradiations prior to the direct detection of ^{1}H decoupled ^{15}N (or ^{13}C) signals. PISEMA relies on off-resonance irradiation to precisely define the "magic angle" [16] for homonuclear $^{1}H/^{1}H$ decoupling, therefore, it is inherently quite sensitive to frequency offsets among the ^{1}H resonances, and these are larger (in kHz) at high fields due to the

* Corresponding author. Fax: +1 858 822 4821.
E-mail address: sopella@ucsd.edu (S.J. Opella).

1090-7807/$ - see front matter © 2007 Elsevier Inc. All rights reserved.
doi:10.1016/j.jmr.2007.10.002

greater spread of chemical shift frequencies. To address this issue, we developed SAMMY [17] and SAMPI4 [18] as magic-sandwich [19,20] based pulse sequences for SLF spectroscopy with on-resonance irradiations that are less susceptible to offset effects. This is now an active research area, and a variety of high resolution SLF experiments have been developed by other groups [21–23] and have been reviewed [11]. It is now possible to select among experiments that are optimized for single crystal, powder, liquid crystal, or aligned biopolymer samples. However, all of these experiments have in common the detection of ^{1}H decoupled ^{15}N (or ^{13}C) signals, which provides chemical shift frequencies in the direct dimension, as in the original double-resonance and SLF experiments.

Fig. 1 compares the timing diagrams for three SLF pulse sequences and the corresponding two-dimensional spectra obtained under identical experimental conditions. The sample is a single crystal of ^{13}Cα, ^{15}N labeled *N*-acetyl-leucine; since there are four uniquely aligned molecules in each unit cell, the spectra have four resonances for each labeled ^{15}N amide site. Because this sample has directly bonded ^{13}C and ^{15}N nuclei, ^{13}C irradiation is applied in the appropriate intervals to yield fully decoupled spectra; this is not needed for experiments performed on samples where only the nitrogen sites are isotopically labeled. Complete two-dimensional spectra are shown in the figures to illustrate the experimental results from application of the pulse sequences. However, the unique spectroscopic information is contained in half of each spectrum, which is symmetric about the zero frequency in the heteronuclear dipole–dipole coupling dimension.

One-dimensional slices through the ^{15}N chemical shift and ^{1}H–^{15}N heteronuclear dipole–dipole coupling frequency dimensions for all four resonances are shown in Fig. 2. All of the frequency axes are adjusted for the scaling factors of the pulse sequences so that the frequencies and linewidths can be directly compared. The order of the individual slices in each panel in Fig. 2 corresponds to the order of resonances with decreasing ^{1}H–^{15}N heteronuclear dipole–dipole coupling frequencies in Fig. 1b, d, and f. Panels a–c in Fig. 2 are ^{15}N chemical shift slices and Panels d–f are heteronuclear dipole–dipole coupling slices taken from the same data sets that are presented as two-dimensional contour plots in Fig. 1.

For comparison, the ^{15}N-detected PISEMA pulse sequence (Fig. 1a), which yields spectra with the narrowest linewidths in the heteronuclear dipolar coupling frequency dimension, was used to obtain the experimental spectrum shown in Fig. 1b. Only three out of the four expected resonances are present in this two-dimensional contour plot because of the broader linewidth and correspondingly reduced intensity of one of the resonances (bottom slices in Fig. 2a and d). This is a typical issue with PISEMA spectra because the strong offset dependence of the Lee–Goldburg irradiation used to suppress the homonuclear ^{1}H/^{1}H dipole–dipole couplings during the heteronuclear spin-exchange interval makes it impossible to have optimal performance for all of the sites when the ^{1}H resonances are spread over a broad range of chemical shift frequencies.

The pulse sequence for ^{15}N-detected PISEMO (Fig. 1c) differs from that for PISEMA (Fig. 1a) in that it uses semi-windowless WaHuHa instead of continuous flip-flop Lee–Goldburg off-resonance irradiation [24] to effect ^{1}H/^{1}H homonuclear decoupling during heteronuclear ^{1}H–^{15}N spin-exchange.

The four pulses labeled P1, P2, P3, and P4 constitute a semi-windowless WaHuHa [3] cycle. The phase P1 is the same as that of the preceding spin-lock irradiation, and the phase of P5 differs by 180°. The phases applied during the even numbered t_1 intervals are the inverse of the phases in the odd numbered t_1 intervals. The durations of the pulses correspond to a nominal nutation angle of 116° [25]. In practice, the phases of P1, P2, P3, P4, P5, P6 are Y, X, $-X$, $-Y$, $-Y$, Y, respectively, for the odd numbered t_1 cycles; and $-Y$, $-X$, X, Y, Y, $-Y$, respectively, for the even numbered t_1 cycles. To suppress the effects of probe ringing in ^{15}N-detected PISEMO, the phase of the first ^{1}H 90° pulse is alternated between X and $-X$, and the corresponding receiver phase is alternated between X and $-X$. In the ^{1}H detected version, the phase of the first ^{1}H 90° pulse is kept constant while the phase of P0 is alternated between X and $-X$, and the alternation of the phase of P_S between X and Y is used to achieve quadrature detection.

The homonuclear decoupling pulse sequence used for ^{1}H detection must fulfill two basic criteria. First, it must have at least one detection window without RF irradiation, which rules out FSLG [24], BLEW12 [26], and other windowless sequences, such as those used in PISEMA [13] and HIMSELF [23] experiments. It is possible to introduce very short detection windows in PISEMA sequences [11], however, in our experience line broadening and loss of sensitivity occur even with the shortest windows (3 μs) that allow sampling on our instruments. Second, the ^{1}H magnetization must be in the transverse plane during the period of the window. The ^{1}H magnetization is along the Z-axis during the windows of SAMMY [17] or SAMPI4 [18], which would otherwise be suitable for this purpose. WaHuHa is effective in this role, since the ^{1}H magnetization is in the transverse plane during the window used to detect the signals as they evolve under the influence of the heteronuclear dipole–dipole coupling. The timing diagrams for the ^{1}H-detected (Fig. 1e) and ^{15}N-detected (Fig. 1c) versions of PISEMO differ only in the placement of the ^{15}N chemical shift evolution period (t_1 in Fig. 1e vs. t_2 in Fig. 1c). Heteronuclear spin-exchange occurs during the t_2 period of ^{1}H-detected PISEMO; the homonuclear decoupling required for high resolution is effected by a multiple-pulse cycle that incorporates windows without irradiation between two of the four pulses. One of the windows is used for data acquisition. The ^{1}H signals are sampled stroboscopically once per cycle to monitor the evolution of the exchange of magnetization between ^{15}N and ^{1}H. The experimental spectra obtained with

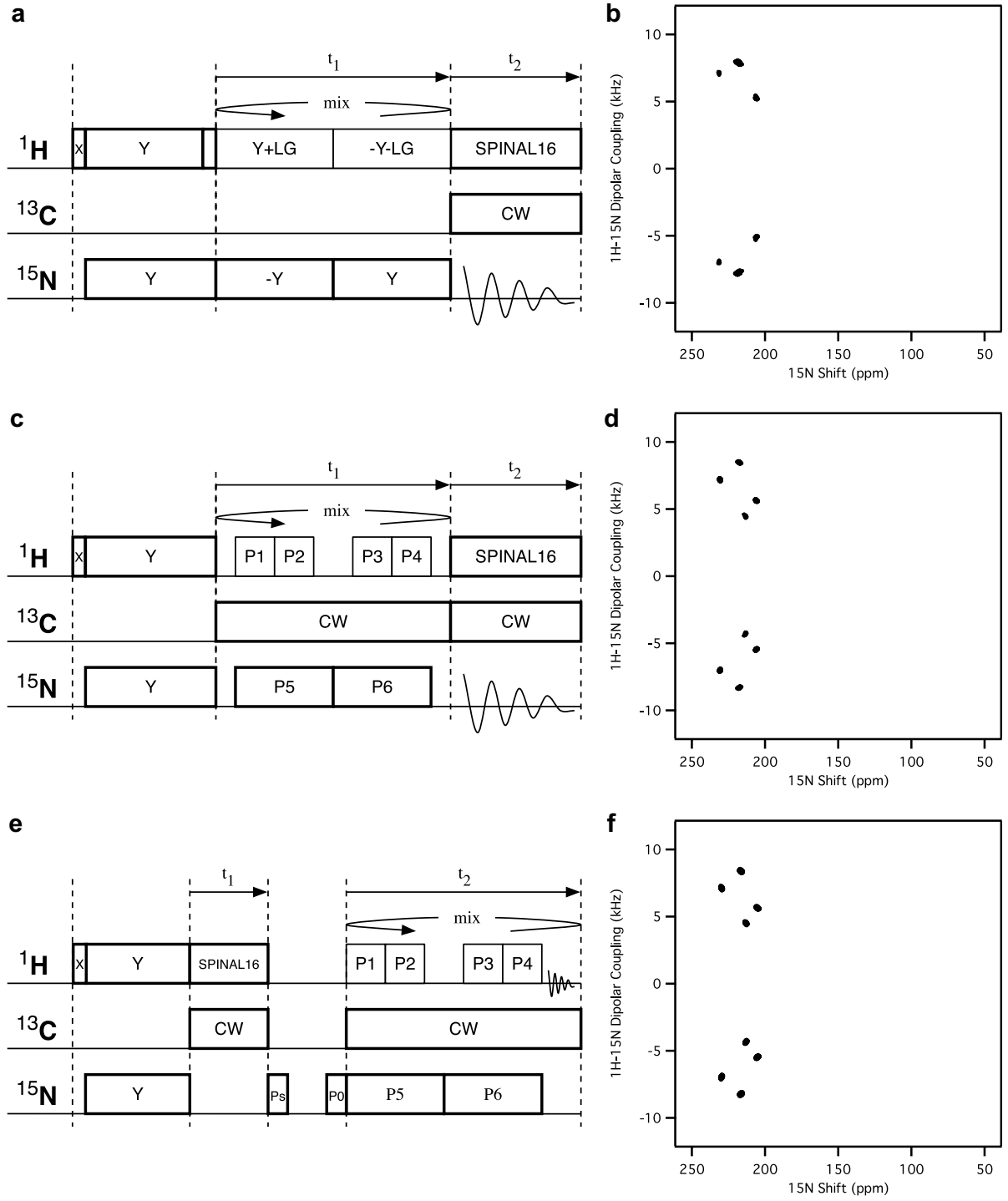

Fig. 1. Timing diagrams for pulse sequences (left column) and the corresponding two-dimensional SLF spectra of a single-crystal of a model peptide (right column). (a and b) ^{15}N-detected PISEMA. (c and d) ^{15}N-detected PISEMO. (e and f) ^{1}H-detected PISEMO. CW refers to continuous wave irradiation. SPINAL-16 refers to modulated irradiation [34,35]. The sample is a single crystal of ^{13}Cα, ^{15}N labeled *N*-acetyl-leucine at an arbitrary orientation. A triple-tuned ^{1}H, ^{13}C, ^{15}N homebuilt probe with a single 5 mm ID solenoid coil was utilized. The Bruker Avance II console was interfaced with a Chemagnetics 500 MHz power amplifier and a homebuilt transmit/receive switch with crossed diodes and a $\lambda/4$ coaxial cable was utilized for ^{1}H detection. For ^{15}N detection, the preamplifier module supplied by Bruker was utilized. In all experiments, the measured $B1$ was 55.6 kHz for all three channels (^{1}H, ^{13}C, and ^{15}N). This corresponds to a 90° pulse of 4.5 μs and 5.8 μs for 116° pulse. For the data shown in (b), the cycle time is 29.2 μs and the jump frequency is ±39544.5 Hz. For the data shown in (d and e), the cycle time is 34.8 μs, which is 6 times the duration of the 116° pulse. The scaling factor for PISEMA is 0.82. The corresponding scaling factor for PISEMO was experimentally determined to be 0.67. For ^{1}H-detected PISEMO, 16 scans, 256 t_1 were acquired with dwell time of 40 μs and 34.8 μs in the t_1 and t_2 dimensions, respectively. For the ^{15}N-detected PISEMA and PISEMO experiments, 32 scans, 256 t_1 were acquired. The dwell times were 29.2 μs and 40 μs in the t_1 and t_2 dimensions. For the PISEMO experiments, the dwell times were 34.8 μs and 40 μs in the t_1 and t_2 dimensions. The number of scans averaged ^{15}N-detected PISEMO spectrum was twice that of the ^{1}H-detected PISEMO spectrum to account for the fact that real and imaginary components of the ^{15}N shift dimension were acquired separately.

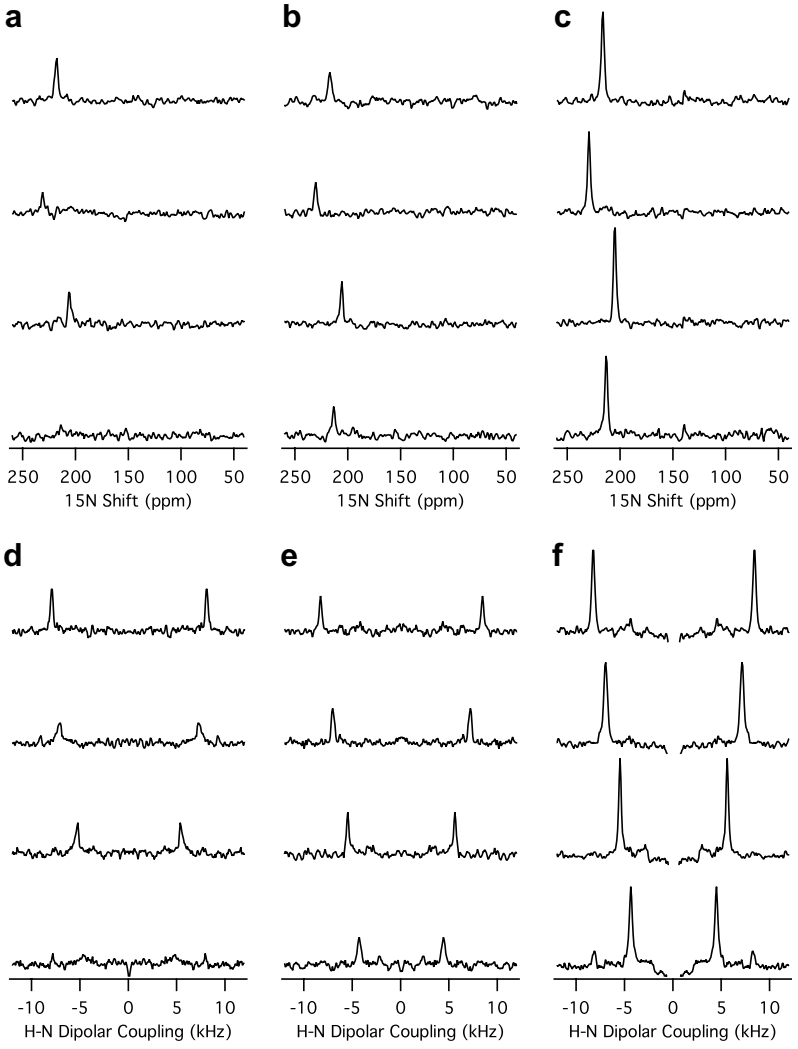

Fig. 2. One-dimensional spectral slices through the resonances in the two-dimensional spectra shown in Fig. 1. (a and d) ^{15}N-detected PISEMA. (b and e) ^{15}N-detected PISEMO. (c and f) ^{1}H detected PISEMO. To allow comparison of the signal-to-noise ratios, the standard deviation was calculated from a section of two-dimensional data that contained only noise, and the data were scaled by their respective standard deviations.

^{1}H-detected PISEMO and ^{15}N-detected PISEMO are essentially identical, except that the ^{1}H-detected version yields signals whose individual signal to noise ratios are between 2.2- and 2.7-fold higher in spectra obtained in the same amount of time. This is shown in the comparison of the one-dimensional slices in Fig. 2.

The principal reason for performing ^{1}H-detected experiments is to gain sensitivity. Following Hong and Yamaguchi [10], we use Eq. (1) to predict the signal-to-noise ratio improvement of ^{1}H-detection compared to ^{15}N-detection in solid-state NMR experiments.

$$\zeta = u(f/2.828)(\gamma_H/\gamma_N)^{3/2}(W_N/W_H)^{1/2}(Q_H/Q_N)^{1/2}(\eta_H/\eta_N) \times (SW_H/FW_H)^{1/2}. \quad (1)$$

ζ is the signal enhancement factor; f is the CP transfer efficiency; γ and W are the gyromagnetic ratios and the line widths in Hz, respectively, for the indicated nuclei (H and N); Q and η are the probe quality factor and the sample filling factor, respectively; SW_H is the ^{1}H spectral width and FW_H is the filter bandwidth. The factor u accounts for ^{15}N-detected PISEMO starting with full ^{15}N magnetization and the ^{1}H-detected version starting with no ^{1}H magnetization. This factor has the effect of reducing the signal enhancement by 0.5. The factors $(\gamma_H/\gamma_N)^{3/2}$, $(W_N/W_H)^{1/2}$ and f are 31.6, 1, and 1, respectively, since the linewidths in the ^{1}H–^{15}N dipole–dipole coupling frequency dimension are about 150 Hz compared to the 3 ppm linewidths observed in the ^{15}N chemical shift frequency dimension; cross-polarization transfer is part of the detection procedure and does not affect the relative sensitivity.

The factor $(SW_H/FW_H)^{1/2}$ is determined, in practice, by the recovery time of the probe following a pulse, and how many data points can be sampled during the duration of the window. The bandwidth of the filter can be adjusted experimentally for a particular probe and window length, or during post-processing with data sampled as fast as possible inside the available window after discarding distorted

data points at the start and end of the period. The experimental spectra in Figs. 1 and 2 resulted from sampling for 2.8 μs out of the total cycle time of 34.8 μs, and the factor $(SW_H/FW_H)^{1/2}$ is calculated as $(2.8/34.8)^{1/2} = 0.28$.

The factors containing Q and η reflect the performance of the two channels of a triple-resonance probe, and can be evaluated using the principle of reciprocity. The 90° pulse length is a direct measure of the signal-to-noise ratio obtainable from a single coil that is used for both transmission and receiving. The magnitude of the $B1$ field is described by Eq. (2) [27]:

$$B1 \text{ (in Hz)} \sim v * H1 \text{ (in Gauss)} \sim (PQv/V)^{1/2}. \quad (2)$$

The power required to achieve the Hartmann–Hahn match condition can be readily measured. In our homebuilt probe, which utilizes a single solenoid coil triple-tuned for ^{1}H at 500 MHz, and ^{13}C and ^{15}N at their corresponding resonance frequencies; 17 W in the ^{1}H channel and 511 W in the ^{15}N channel provides $B1$ fields of 55.6 kHz. The calculated probe performance difference is $(Q_H V_N/Q_N V_H)^{1/2} = (P_N v_N/P_H v_H)^{1/2} = 1.8$. This is essentially the same as that based on the Q_H of 220 and Q_N of 70 measured with a network analyzer. For other types of probes, such as those utilizing cross-coils, measuring the Q alone will not be sufficient to determine the probe-related factors affecting sensitivity [28]. In our experience, measuring the $B1$ field is a simple and reliable approach to characterizing the probe.

Combining all the factors that affect the signal-to-noise ratio, we predict an enhancement factor $\zeta = 2.8 = 0.5 \times 0.35 \times 31.6 \times 1.0 \times 1.8 \times 0.28$, which is in remarkably good agreement with the experimentally observed enhancement factors for the four individual resonances between 2.2 and 2.7.

The ^{1}H-detected PISEMO spectrum of a single crystal in Fig. 1e provides a significant improvement in sensitivity compared to the equivalent ^{15}N-detected experiment. The signal to noise ratio can be further improved through the use of a preamplifier and radiofrequency switching system that is optimized for observing the ^{1}H frequencies; additional improvements may come from an increase of the number of data points acquired in the windows used for stroboscopic detection and optimization of both the analog and digital filters in the spectrometer. Further improvements in the sensitivity of solid-state NMR experiments performed on samples of proteins and other biopolymers in lossy aqueous solutions can result from the increased efficiency and homogeneity of the ^{1}H channel and reduced sample heating that result from the use of "low-E" coils [29–32]. Because these probes often sacrifice efficiency on the low frequency channels, their optimal implementation may be for ^{1}H-detected experiments at high fields.

Not only does ^{1}H-detected PISEMO yield SLF spectra with improved sensitivity compared to the equivalent ^{15}N-detected experiment, but also it provides a building block for more sophisticated pulse sequences [33] because of its favorable bandwidth for heteronuclear spin-exchange and the added flexibility that results from the ability to detect free induction decays that reflect the evolution of dipole–dipole coupling rather than chemical shift frequencies.

Acknowledgments

We thank A.A. Nevzorov and C.V. Grant for helpful discussions, and N. Sinha for providing the sample. This research was supported by Grants RO1EB001966 and RO1GM075877 from the National Institute of Health, and utilized the Resource of NMR Molecular Imaging of Proteins, which is supported by Grant P41EB002031.

References

[1] S.R. Hartman, E.L. Hahn, Nuclear double resonance in the rotating frame, Phys. Rev. 128 (1962) 2042–2053.
[2] A. Pines, M.G. Gibby, J.S. Waugh, Proton-enhanced nuclear induction spectroscopy. A method for high resolution NMR of dilute spins in solids, J. Chem. Phys. 56 (1972) 1776–1777.
[3] J.S. Waugh, L.M. Huber, U. Haeberlen, Approach to high-resolution NMR in solids, Phys. Rev. Lett. 20 (1968) 180–182.
[4] Y. Ishii, R. Tycko, Sensitivity enhancement in solid state ^{15}N NMR by indirect detection with high-speed magic angle spinning, J. Magn. Reson. 142 (2000) 199–204.
[5] B. Reif, R.G. Griffin, ^{1}H detected ^{1}H,^{15}N correlation spectroscopy in rotating solids, J. Magn. Reson. 160 (2003) 78–83.
[6] C.R. Morcombe, E.K. Paulson, V. Gaponenko, R.A. Byrd, K.W. Zilm, ^{1}H–^{15}N correlation spectroscopy of nanocrystalline proteins, J. Biomol. NMR 31 (2005) 217–230.
[7] V. Chevelkov, K. Rehbein, A. Diehl, B. Reif, Ultrahigh resolution in proton solid-state NMR spectroscopy at high levels of deuteration, Angew. Chem. Int. Ed. 45 (2006) 3878–3881.
[8] D.H. Zhou, D.T. Graesser, W.T. Franks, C.M. Rienstra, Sensitivity and resolution in proton solid-state NMR at intermediate deuteration levels: quantitative linewidth characterization and applications to correlation spectroscopy, J. Magn. Reson. 178 (2006) 297–307.
[9] D.H. Zhou, G. Shah, M. Cormos, C. Mullen, D. Sandoz, C.M. Rienstra, Proton-detected solid-state NMR spectroscopy of fully protonated proteins at 40 kHz magic-angle spinning, J. Am. Chem. Soc. 129 (2007) 11791–11801.
[10] M. Hong, S. Yamaguchi, Sensitivity-enhanced static ^{15}N NMR of solids by ^{1}H indirect detection, J. Magn. Reson. 150 (2001) 43–48.
[11] A. Ramamoorthy, Y. Wei, D.K. Lee, PISEMA solid-state NMR spectroscopy, Ann. Rep. NMR Spectrosc. 52 (2004) 1–52.
[12] J.S. Waugh, Uncoupling of local field spectra in nuclear magnetic resonance: determination of atomic positions in solids, Proc. Natl. Acad. Sci. USA 73 (1976) 1394–1397.
[13] C.H. Wu, A. Ramamoorthy, S.J. Opella, High-resolution heteronuclear dipolar solid-state NMR spectroscopy, J. Magn. Reson. A109 (1994) 270–272.
[14] R.K. Hester, J.L. Ackerman, B.L. Neff, J.S. Waugh, Separated local field spectra in NMR: determination of structure of solids, Phys. Rev. Lett. 36 (1976) 1081–1083.
[15] S.J. Opella, J.S. Waugh, Two-dimensional ^{13}C NMR of highly oriented polyethylene, J. Chem. Phys. 66 (1977) 4919–4924.
[16] W.I. Goldburg, M. Lee, Nuclear magnetic resonance line narrowing by a rotating RF field, Phys. Rev. Lett. 11 (1963) 255–258.
[17] A.A. Nevzorov, S.J. Opella, A "Magic Sandwich" pulse sequence with reduced offset dependence for high-resolution separated local field spectroscopy, J. Magn. Reson. 164 (2003) 182–186.
[18] A.A. Nevzorov, S.J. Opella, Selective averaging for high-resolution solid-state NMR spectroscopy of aligned samples, J. Magn. Reson. 185 (2007) 59–70.

[19] W.K. Rhim, A. Pines, J.S. Waugh, Time-reversal experiments in dipolar-coupled spin systems, Phys. Rev. B3 (1971) 684–696.
[20] K. Takegoshi, C.A. McDowell, A "Magic Echo" pulse sequence for the high-resolution NMR spectra of abundant spins in solids, Chem. Phys. Lett. 116 (1985) 100–104.
[21] K. Schmidt-Rohr, D. Nanz, L. Emsley, A. Pines, NMR measurement of resolved heteronuclear dipole couplings in liquid crystals and lipids, J. Phys. Chem. 98 (1994) 6668–6670.
[22] S.V. Dvinskikh, H. Zimmermann, A. Maliniak, D. Sandstrom, Separated local field spectroscopy of columnar and nematic liquid crystals, J. Magn. Reson. 163 (2003) 46–55.
[23] S.V. Dvinskikh, K. Yamamoto, A. Ramamoorthy, Heteronuclear isotropic mixing separated local field NMR spectroscopy, J. Chem. Phys. 125 (2006) 034507.
[24] A. Bielecki, A.C. Kolbert, H.J.M. DeGroot, R.G. Griffin, M.H. Levitt, Frequency-switched Lee–Goldburg sequences in solids, Adv. Magn. Reson. 14 (1990) 111–124.
[25] U. Haeberlen, High resolution NMR in solids: selective averaging, Adv. Magn. Reson. 114 (1976).
[26] D.P. Burum, M. Linder, R.R. Ernst, Low-power multipulse line narrowing in solid-state NMR, J. Magn. Reson. 44 (1981) 173–188.
[27] E. Fukushima, S.B.W. Roeder, Experimental pulse NMR, a nuts and bolts approach, Addison-Wesley, 1981, pp.539.
[28] D.I. Hoult, R.E. Richards, The signal-to-noise ratio of the nuclear magnetic resonance experiment, J. Magn. Reson. 24 (1976) 71–85.
[29] J.A. Stringer, C.E. Bronniman, C.G. Mullena, D.H. Zhoub, S.A. Stellfoxb, Y. Lib, E.H. Williams, C.M. Rienstra, Reduction of RF-induced sample heating with a scroll coil resonator structure for solid-state NMR probes, J. Magn. Reson. 173 (2005) 40–48.
[30] F.D. Doty, J. Kulkarni, C. Turner, G. Entzminger, A. Bielecki, Using a cross-coil to reduce RF heating by an order of magnitude in triple-resonance multinuclear MAS at high fields, J. Magn. Reson. 182 (2006) 239–253.
[31] P. Gor'kov, E.Y. Chekmenev, C. Li, M. Cotten, J.J. Buffy, N.J. Traaseth, G. Veglia, W.W. Brey, Using low-E resonators to reduce RF heating in biological samples for static solid-state NMR up to 900 MHz, J. Magn. Reson. 185 (2007) 77–93.
[32] C.V. Grant, S.L. Sit, A.A. DeAngelis, K.S. Khuong, C.H. Wu, L.A. Plesniak, S.J. Opella, An efficient $^{1}H/^{31}P$ double-resonance solid-state NMR probe that utilizes a scroll coil, J. Magn. Reson. 188 (2007) 279–284.
[33] C.H. Wu, S.J. Opella, Shiftless NMR spectroscopy, J. Chem. Phys., in press.
[34] B.M. Fung, A.K. Khitrin, K. Ermolaev, An improved broadband decoupling sequence for liquid crystals and solids, J. Magn. Reson. 142 (2000) 97–101.
[35] N. Sinha, C.V. Grant, C.H. Wu, A.A. DeAngelis, S.C. Howell, S.J. Opella, SPINAL modulated decoupling in high field double- and triple-resonance solid-state NMR experiments on stationary samples, J. Magn. Reson. 177 (2005) 197–202.